The Astrophysical Journal, 810:82 (15pp), 2015 September 1 doi:10.1088/0004-637X/810/1/82

SCATTER-DOMINATED INTERPLANETARY TRANSPORT OF SOLAR ENERGETIC PARTICLES IN LARGE GRADUAL EVENTS AND THE FORMATION OF DOUBLE POWER-LAW DIFFERENTIAL FLUENCE SPECTRA OF GROUND-LEVEL EVENTS DURING SOLAR CYCLE 23

Gen Li and Martin A. Lee
Space Science Center, Institute for the Study of Earth, Oceans, and Space, University of New Hampshire, Durham, NH 03824, USA; gjk44@wildcats.unh.edu
Received 2015 February 14; accepted 2015 July 24; published 2015 September 1

ABSTRACT

The effects of scatter-dominated interplanetary transport on the spectral properties of the differential fluence of large gradual solar energetic particle (SEP) events are investigated analytically. The model assumes for simplicity radial constant solar wind and radial magnetic field. The radial diffusion coefficient is calculated with quasilinear theory by assuming a spectrum of Alfvén waves propagating parallel to the magnetic field. Cross-field transport is neglected. The model takes into consideration several essential features of gradual event transport: nearly isotropic ion distributions, adiabatic deceleration in a divergent solar wind, and particle radial scattering mean free paths increasing with energy. Assuming an impulsive and spherically symmetric injection of SEPs with a power-law spectrum near the Sun, the predicted differential fluence spectrum exhibits at 1 AU three distinctive power laws for different energy domains. The model naturally reproduces the spectral features of the double power-law proton differential fluence spectra that tend to be observed in extremely large SEP events. We select nine western ground-level events (GLEs) out of the 16 GLEs during Solar Cycle 23 and fit the observed double power-law spectra to the analytical predictions. The compression ratio of the accelerating shock wave, the power-law index of the ambient wave intensity, and the proton radial scattering mean free path are determined for the nine GLEs. The derived parameters are generally in agreement with the characteristic values expected for large gradual SEP events.

Key words: acceleration of particles – interplanetary medium – Sun: particle emission

1. INTRODUCTION

Solar energetic particle (SEP) events are commonly classified into two categories: the so-called large "gradual" events, in which the primary accelerators are shocks driven by fast coronal mass ejections (CMEs), and small "impulsive" events, in which particles are accelerated at sites associated with flares. Compared with impulsive events, gradual events are generally more intense, long-lasting events that inject SEPs over a much broader range of longitudes. Gradual events are of great practical importance since they are responsible for most space weather disturbances of Earth's magnetosphere and upper atmosphere. The shock origin also makes gradual events productive opportunities for refining our understanding of shock acceleration and particle transport.

At a CME-driven shock, ions are injected into the shock acceleration process. Upstream of the shock, hydromagnetic waves are exited at the resonant frequencies owing to a streaming instability driven by the accelerating protons that attempt to escape upstream with a super-Alfvénic streaming velocity (Bell 1978). The excited upstream waves advect through the shock to the downstream plasma, where they are compressed and further enhanced. Such a wave enhancement creates a turbulent sheath that traps the ions near the shock and promotes effective diffusive shock acceleration (Lee 1983; Reames & Ng 1998; Gordon et al. 1999; Vanio et al. 2000). In the sheath, proton-excited waves produce the short scattering mean paths essential for SEPs to be accelerated sufficiently rapidly to overcome adiabatic deceleration, upstream escape possibilities, and limited acceleration time. The scatter-dominated ions may be accelerated up to ∼10 GeV by a combination of the first-order Fermi process and shock drift acceleration (Jokipii 1982). In gradual events, the particles first observed are those that escape from the turbulent sheath with the help of the outward magnetic mirror force associated with the interplanetary magnetic field and stream nearly scatter-free to Earth orbit. After the shock weakens significantly or passes Earth orbit, particles eventually fill the inner heliosphere through enhanced diffusion due to the decaying turbulence, while they adiabatically cool in the solar wind.

The power-law spectrum of the accelerated ions is one of the essential properties of planar stationary diffusive shock acceleration for ion injection at low energies. At high energies for nonplanar or time-dependent shocks, the spectrum is expected to be modified by an exponential rollover as a result of particle losses by escape, particle adiabatic deceleration, or limited shock lifetime. In gradual events, ion spectra observed at 1 AU clearly evolve with time (Tylka et al. 2000, 2005). However, observations of event-averaged/integrated SEPs for many species over a broad energy range (∼0.1 to ∼100 MeV/nuc) during Solar Cycle 23 reveal that large SEP events usually have power-law spectra below a few MeV/nuc followed by spectral breaks or rollovers at higher energies (Cohen et al. 2005; Mewaldt et al. 2005, 2008; Tylka et al. 2005). In studies of the five large SEP events during 2003 October–November, Mewaldt et al. (2005) suggested that a double power-law form did a better job of fitting the differential fluence spectra than the "power law × exponential" spectral form proposed by Ellison & Ramaty (1985).

In some of the largest gradual SEP events, the intensity of GeV protons is sufficiently large to rise detectably at ground level above the galactic cosmic-ray background. These events are known as ground-level events (GLEs). Mewaldt et al. (2012) found that, from ∼0.1 MeV to several hundred MeV, the proton differential fluence spectra of all 16 GLE events during Solar Cycle 23 can be well fitted by a double power-law

Table 1
Selected Properties of the 16 GLE Events of Solar Cycle 23[a]

Date	Location	E_0 (MeV)	γ_1	γ_2	Fe/O 12–45 MeV/n	Fe/O 45–80 MeV/n
1997 Nov 06	S18W63	91.3	1.56	2.44	0.733	0.765
1998 May 02	S15W15	114	1.86	2.83	0.683	0.674
1998 May 06	S11W65	3.81	0.94	2.58	0.531	0.294
1998 Aug 24	N35E09	10.6	1.35	3.85	0.018	0.863
2000 Jul 14	N22W07	24.2	1.09	3.80	0.099	0.106
2001 Apr 15	S20W85	16.1	1.23	2.24	0.486	0.813
2001 Apr 18	S23W117	19.9	1.31	2.51	0.186	0.519
2001 Nov 04	N06W18	25.4	1.19	4.53	0.067	0.038
2001 Dec 26	N08W54	31.7	1.53	3.14	0.412	0.671
2002 Aug 24	S02W81	14.5	1.25	2.90	0.222	0.824
2003 Oct 28	S20E02	27.0	1.03	4.41	0.041	0.006
2003 Oct 29	S19W09	27.7	1.11	2.94	0.141	0.126
2003 Nov 02	S18W59	13.3	1.09	3.46	0.043	0.118
2005 Jan 17	N14W25	40.5	1.54	4.63	0.031	0.010
2005 Jan 20	N14W61	8.18	0.97	2.14	0.198	0.188
2006 Dec 13	S06W23	3.01	0.82	2.42	0.778	0.804

Note.
[a] All the data in Table 1 are from Mewaldt et al. (2012).

form (Band et al. 1993) as

$$dF/dE = CE^{-\gamma_1}\exp\left(-E/E_0\right) \text{ for } E \leqslant (\gamma_2 - \gamma_1)E_0;$$
$$dF/dE = CE^{-\gamma_2}\left[(\gamma_2 - \gamma_1)E_0\right]^{(\gamma_2-\gamma_1)} \times \exp(\gamma_1 - \gamma_2) \text{ for } E \geqslant (\gamma_2 - \gamma_1)E_0, \quad (1)$$

where F is fluence, E is kinetic energy, C is a normalization constant, γ_1 is the low-energy power-law slope, γ_2 is the high-energy power-law slope, and E_0 is the break energy. At higher energies ($\sim$0.5 GeV), GLE spectra typically steepen further. The purpose of this paper is to account for the form of the differential fluence spectra of these 16 events. Selected properties and relevant parameters of the events are listed in Table 1.

Because of the unique parameters describing the shock acceleration and interplanetary transport of each gradual event, it is quite intractable to give a universal description of what determines the spectral variability. The SEPs observed throughout a gradual event arise from a sequence of different magnetic flux tubes. In each magnetic flux tube, the distribution of SEPs results from a superposition of the transport-modulated ions injected at the moving shock. At an evolving CME-driven shock near the Sun, the shock obliquity, the compression ratio, and the important transport parameters may change rapidly with time (t) and heliocentric radial distance (r). At an interplanetary shock where the shock parameters become relatively stable owing to its large spatial scale, the shock obliquity and the particle intensity at the shock front can still be affected by some subtle factors such as local variations in solar wind parameters and the resulting shock front warps (Neugebauer & Giacalone 2005). It is worth noting that the magnetic field morphology may also vary from event to event. A well-analyzed example is the 2001 September 24 event, in which the interplanetary magnetic field lines were draped around the flank of the preceding CME that was launched 3 days before the primary CME. The field lines compressed at the nose of the preceding CME formed a "magnetic bottleneck" and served as a transient reflecting boundary for interplanetary transport of SEPs (Tan et al. 2008).

Though numerous uncertainties are involved in the formation of the SEP spectra of gradual events, several global factors have been systematically analyzed and applied to interpret the observed spectral features:

1. Cane et al. (1986, 2003, 2006) suggested that interplanetary shocks are the controlling agents for the asymmetric distribution of SEPs in longitude. As a result, SEP intensity-time profiles can be organized as a function of the heliolongitude of the associated flare. Western events tend to have a prompt onset followed by a gradual decay, while eastern events usually increase slowly, followed by the peaking of ion intensities at the passage of the associated interplanetary shock; central meridian events show intermediate profiles. One evident influence of interplanetary shock acceleration on SEP spectra is that locally accelerated populations steepen the proton spectra and reduce the Fe/O ratio at energies of tens of MeV/nuc (Cane et al. 1986, 2003).
2. Reames (1990) found that many large events have an intensity plateau caused by the regulation of ion escape from the vicinity of the shock by proton-excited waves. At a traveling shock where the shock strength remains high, the proton-excited waves diffusively trap ions and limit the fraction of ions that escape the shock upstream, throttling the SEP intensities at the "streaming limit" (Ng & Reames 1994; Ng et al. 2003; Vainio 2003; Lee 2005). Reames & Ng (2010) showed that, in some of the largest GLEs, ion spectra at low energies (<10 MeV/nuc) are strongly suppressed in the plateau phase. They suggested that the suppression is due to the resonance of low-energy ions with the intense waves generated by higher-energy protons that have preceded them in the upstream region.
3. Tylka & Lee (2006) proposed a shock-geometry hypothesis in which flare seed particles are favored over those injected out of the thermal or suprathermal solar wind at quasi-perpendicular shocks, whereas the reverse is the

case at quasi-parallel shocks. By averaging the differential intensity of shock-accelerated ions over different ranges of the shock normal angle, they reproduced the key spectral and compositional characteristics above ~1 MeV/nuc.

There is no doubt that all the factors mentioned above contribute to shaping the proton differential fluence spectra of the 16 GLE events of Solar Cycle 23. Nevertheless, in this paper we focus on the role of interplanetary propagation in determining the observed properties of the differential fluence spectra. Compared with ordinary gradual events, GLEs are presumably better probes of shock acceleration close to the Sun where particles achieve higher energies; these particles spend sufficient time in interplanetary space before they arrive at Earth orbit to reveal the effects of interplanetary transport. Gopalswamy et al. (2012) showed that, in all of the 16 GLE events, the CME height at the time of the metric type II burst is ~1.5 solar radii from Sun center, where the shock acceleration is extremely rapid owing to the strong magnetic field. Mewaldt et al. (2012) found that GLEs have significantly harder spectra above the break energy than large non-GLE events and that 9 of the 16 GLEs are Fe-rich in the 45–80 MeV/nuc interval. Six of the nine events have the associated flare location between W20 and W90, which generally implies optimal magnetic connection between the observer and the particle sources in the low corona. These observations may be evidence that the proton fluence of well-connected GLE events is dominated at energies above tens of MeV by populations accelerated near the Sun.

The goal of this work is to account for the formation of the double power-law spectrum with a power-law source characteristic of shock acceleration and scatter-dominated transport described by the Parker transport equation (Parker 1965a). In Section 2, we present the mathematical description of the differential fluence. We show that, through transport modulation, SEPs with a single power-law spectrum released close to the Sun exhibit at 1 AU three different spectral slopes depending on their energy. In Section 3, we select nine events out of the 16 GLEs during Solar Cycle 23. The selected events are generally western Fe-rich events, presumably less influenced by the extended acceleration at interplanetary shocks than near-central meridian GLEs. We fit the observed proton differential fluence spectra of the nine GLEs to the analytical predictions. We find that the derived compression ratio of the accelerating shock wave, the power-law index of the ambient wave intensity, and the proton radial scattering mean free path are generally reasonable; the model is successful in accounting for the observed spectral features. In Section 4 we enumerate the limitations of the model and discuss the influence of diffusive shock acceleration in interplanetary space on the SEP spectra observed in near-central meridian GLEs. In Section 5 we summarize our conclusions.

2. THE MODEL

2.1. Governing Equations

Ion transport in ambient solar wind is conventionally characterized by low wave intensities in the resonant frequency range and by large scattering mean free paths parallel to the ambient magnetic field. However, in large gradual events, particle streaming tends to decrease rapidly within a few hours of the event onset, and ion anisotropies are generally small after an initial increase (Reames et al. 2001; Tan et al. 2007). Ng et al. (1999, 2003) suggested that the rapid decrease of streaming is due to the local Alfvén-wave growth, which may significantly reduce the scattering mean free paths of ions even near or beyond 1 AU. Mason et al. (2006) also confirmed the existence of strong interplanetary scattering by showing that, for heavy ions at ~10 MeV/nuc, scattering dominates the temporal evolution of the intensities observed at 1 AU. Based on the above studies, we neglect in our model the early phase of SEP events when streaming is large and consider SEPs to be nearly isotropic in large gradual events.

Recent studies (Dalla et al. 2013; Marsh et al. 2013) calculated in detail the drift velocity for protons of 100 MeV as a function of heliocentric radial distance and heliolatitude. Their work pointed out that drift transport in the Archimedes spiral magnetic field can be an effective source of cross-field transport for high-energy SEPs, particularly at large solar radii and high latitudes. Since we focus on the propagation of SEPs between the Sun and 1 AU near the ecliptic plane where the magnetic field is strong and its curvature not significant, we neglect in our model the curvature of the Archimedes spiral magnetic field and drift transport. We consider a radial constant solar wind with speed V_{sw} and a radial mean interplanetary magnetic field $B \propto r^{-2}$. The interplanetary transport of energetic ions on a radial magnetic flux tube is usually treated using the focused transport equation (Roelof 1969; Earl 1976; Ruffolo 1995; Isenberg 1997). We derive in Appendix A that, with sufficient interplanetary scattering, the focused transport equation can be simplified to the following form (Parker 1965a) for SEPs characterized by particle speeds $v \gg V_{sw}$:

$$\frac{\partial f}{\partial t} + V_{sw}\frac{\partial f}{\partial r} - \frac{1}{r^2}\frac{\partial}{\partial r}\left(r^2 K \frac{\partial f}{\partial r}\right) - \frac{2V_{sw}}{3r}p\frac{\partial f}{\partial p} = u_{inj}(r, p, t), \quad (2)$$

where $f(r, p, t)$ is the omnidirectional distribution function of a particular species within a radial flux tube, p is particle momentum magnitude, u_{inj} is a source, and K is the radial diffusion coefficient given by

$$K = \frac{1}{3}\lambda_{MFP} v = \frac{v^2}{8}\int_{-1}^{1} d\mu \frac{1-\mu^2}{D_{\mu\mu}}, \quad (3)$$

where λ_{MFP} is the radial scattering mean free path, μ is the cosine of the particle pitch angle, and $D_{\mu\mu}$ is the pitch angle diffusion coefficient.

Assuming a spectrum of parallel-propagating Alfvén waves, $D_{\mu\mu}$ can be related to interplanetary turbulence through quasilinear theory as (Jokipii 1966; Lee 1982)

$$D_{\mu\mu} = \frac{\pi\Omega^2}{2B^2}\frac{}{|\mu| v} I\left(k = \frac{\Omega}{\mu v}\right), \quad (4)$$

where $\Omega[=QB/(\Gamma Mc)]$ is the particle gyrofrequency, M is particle mass, Q is particle charge, Γ is the particle Lorenz factor, and $I(k)$ is the wave intensity defined in terms of wavenumber k as

$$\left\langle |\delta B|^2 \right\rangle = \int_{-\infty}^{+\infty} dk\, I(k), \quad (5)$$

where δB is the fluctuating value of the interplanetary magnetic field. We take $|\delta B|^2 \propto r^{-3}$ following the WKB model of wave

propagation in the solar wind (Parker 1965b; Hollweg 1973). For the energy range in our study, k is located in the inertial range of solar wind turbulence. Thus, we take

$$I(k) \propto r^{-3} k^{-\eta}, \tag{6}$$

where η is the spectral slope of the wave intensity. From Equations (3), (4), and (6), it can be readily shown that for nonrelativistic particles

$$K(r, p) = K_0 p^{\alpha} r^{\beta}, \tag{7}$$

where $\alpha = 3 - \eta$, $\beta = 3 - 2\eta$, and K_0 is a constant. Presumably the interplanetary magnetic field fluctuations exhibit a Kolmogorov-like spectrum ($\eta \sim 5/3$) in the inertial range. To allow for spectral variation in the inertial range and modifications due to SEP wave excitation, we restrict η to the range $1 < \eta < 2$, i.e., $1 < \alpha < 2$ and $-1 < \beta < 1$.

Notice that Equation (2) applies to a single magnetic flux tube in the absence of drift and diffusive transport normal to the magnetic field, as we have assumed. Throughout an SEP event, a spacecraft samples a series of "corotating" flux tubes that connect the observer to regions of different heliolongitudes in the inner heliosphere. The shock parameters may vary systematically over such a longitude span. To proceed analytically, we assume that K and $u_{\rm inj}$ are spherically symmetric about the Sun, whereby the differential fluence arising from the corotating flux tubes is equivalent to that arising from a single flux tube. This simplification, generally reasonable for well-connected gradual events owing to the usually broad longitude extent of the CME and shock, may be less reliable for poorly connected events since the shock parameters are more sensitively dependent on longitude at the distant flanks than near the nose of the shock. We shall return to this issue in Section 4.

Considering an SEP event that starts at t_1 and ends at t_2, the differential fluence in units of ions cm^{-2} sr^{-1} MeV^{-1} can be written as

$$dF/dE = p^2 \overline{f}\,, \tag{8}$$

where $\overline{f} = \int_{t_1}^{t_2} f dt$. Integrating Equation (2) over $[t_1, t_2]$, we obtain

$$V_{\rm sw}\frac{\partial \overline{f}}{\partial r} - \frac{1}{r^2}\frac{\partial}{\partial r}\left(K_0 p^{\alpha} r^{\beta+2}\frac{\partial \overline{f}}{\partial r}\right) - \frac{2V_{\rm sw}}{3r}p\frac{\partial \overline{f}}{\partial p} = \frac{U}{16\pi^2 r^2 p^2}, \tag{9}$$

where $U(r, p) = 16\pi^2 r^2 p^2 \int_{t_1}^{t_2} u_{\rm inj} dt$ is normalized as $\int_0^r dr' \int_0^p dp' U(r', p') = N$, with $N(r, p)$ being the total number of particles injected within the sphere of heliocentric radius r with momentum magnitude up to p. We have used the condition $f(t_1) = f(t_2) = 0$ since an "event" must start and end with vanishing particle intensity.

The Green's function $G(r, p; r_0, p_0)$ of Equation (9) satisfies

$$V_{\rm sw}\frac{\partial G}{\partial r} - \frac{1}{r^2}\frac{\partial}{\partial r}\left(K_0 p^{\alpha} r^{\beta+2}\frac{\partial G}{\partial r}\right) - \frac{2V_{\rm sw}}{3r}p\frac{\partial G}{\partial p} = \frac{\delta(r - r_0)\delta(p - p_0)}{16\pi^2 r_0^2 p_0^2}. \tag{10}$$

Under the boundary conditions that $G \to 0$ as $r \to \infty$ and that G is finite as $r \to 0$, solutions of Equation (10) are given by Webb & Gleeson (1974): if $\beta \neq 1$,

$$G = \frac{3}{64\pi^2 V_{\rm sw} p_0^3 r_0^2 |j+1|}\left(\frac{R_0}{R}\right)^j \frac{R_0^2}{T} \times \exp\left(-\frac{R^2 + R_0^2}{4T}\right) I_{|j|}\left(\frac{RR_0}{2T}\right), \tag{11}$$

where $R = 2(1-\beta)^{-1}(rp^{3/2})^{(1-\beta)/2}$, $R_0 = R(r_0, p_0)$, $j = (1+\beta)/(1-\beta)$, and $I_{|j|}$ is the modified Bessel function of the first kind, not to be confused with the wave intensity $I(k)$ defined in Equation (5); if $\beta = 1$,

$$G = \frac{3}{64\pi^{5/2} V_{\rm sw} p_0^3 r_0^2}\frac{1}{\sqrt{T}}\exp\left[\frac{-\left(R_0' - R' - 2T\right)^2}{4T}\right], \tag{12}$$

where $R' = -\ln(2^{1/2} r p^{3/2})$ and $R_0' = R'(r_0, p_0)$. In both cases, $T = 3K_0\left(p_0^{\chi} - p^{\chi}\right)(2V_{\rm sw}\chi)^{-1}$ and $\chi = \alpha + (3/2)(1-\beta)$.

The differential fluence can be calculated by convoluting the Green's function with the source function as

$$dF/dE = p^2 \overline{f} = p^2 \int_p^{\infty} dp_0 \int_0^{+\infty} dr_0 U(r_0, p_0) \times G(r, p; r_0, p_0). \tag{13}$$

2.2. Proton Differential Fluence Spectra Arising from a Power-law Source Injected near the Sun

We focus on the proton differential fluence spectra observed at 1 AU for the 16 GLEs in Solar Cycle 23 over the energy range from 0.1 MeV to several hundred MeV. In this energy domain, we assume that the shock may be taken initially to be planar and stationary for proton acceleration since ~GeV protons are usually released soon after CME initiation in GLE events (Kahler 1994; Reames et al. 2001). We consider a simplified scenario in which a proton population is accelerated by a stationary planar shock and injected impulsively at $r = r_s$, where $r_s \ll 1$AU indicates the shock's approximate position. Since the proton differential fluence spectra of all 16 GLEs can be well fitted by a double power-law form, we reasonably assume that, early in a GLE event, the high-energy spectral rollover of the injected protons does not occur within the energy range of our study. Correspondingly, we restrict $U(r, p)$ to have the form

$$U(r, p) \propto p^{-\gamma}\delta(r - r_s), \tag{14}$$

where γ is the power-law index of the shock-accelerated protons. Following the shock acceleration model by Lee (1983), we take $\gamma = 3X(X-1)^{-1} - 2$, with X the shock compression ratio. Although idealized, the impulsive source injection at $r_s \ll 1$AU is not unrealistic for high-energy SEPs in well-connected GLE events: the acceleration efficiency usually decreases rapidly as the shock moves outward and its strength weakens, and Reames (2009) showed that the height of the shock at the time of initial solar particle release is generally below 4 solar radii for western GLEs. At low energies where the diffusive shock acceleration in interplanetary space is not negligible, extended injection of energetic protons should be included in the source term. Consequences of extended acceleration will be addressed later.

Since our objective is to determine the dependence of differential fluence on p and r, we ignore all constant factors in Equation (11) and obtain

$$G(r, p; r_0, g) \propto r^{-(1+\beta)/2} p^{-\alpha-3} g^{\alpha+(3/4)(3-\beta)} \left(1 - g^{\chi}\right)^{-1} \times I_{\frac{1+\beta}{1-\beta}}\left[2C\left(r_0/r\right)^{(1-\beta)/2} g^{\alpha+(3/4)(1-\beta)}\left(1 - g^{\chi}\right)^{-1}\right] \times \exp\left\{-Cg^{\alpha}\left[g^{(3/2)(1-\beta)} + \left(r_0/r\right)^{1-\beta}\right]\left(1 - g^{\chi}\right)^{-1}\right\}, \quad (15)$$

where $C = (2/3)(1 - \beta)^{-2}\chi V_{\rm sw} r K^{-1}$ and $g = p/p_0$ ranging from 0 to 1. From Equations (13)–(15), we have

$$dF/dE \propto r^{-(1+\beta)/2} p^{-\alpha-\gamma} \int_0^1 dg g^{\alpha+\gamma+(1-3\beta)/4}\left(1 - g^{\chi}\right)^{-1} \times I_{\frac{1+\beta}{1-\beta}}\left[Dg^{\alpha+(3/4)(1-\beta)}\left(1 - g^{\chi}\right)^{-1}\right] \times \exp\left\{-Cg^{\alpha}\left[g^{(3/2)(1-\beta)} + \left(r_s/r\right)^{1-\beta}\right]\left(1 - g^{\chi}\right)^{-1}\right\}, \quad (16)$$

where $D = 2(r_s/r)^{(1-\beta)/2} C$.

In Appendix B, we develop an approximate analytical solution for Equation (16) by simplifying and evaluating the integral near g_0 where the integrand is maximized. The solution is

$$\begin{aligned} dF/dE &\propto r^{-1-\beta} p^{-\alpha-\gamma} \\ &\quad \text{if } V_{\rm sw} r/K(r, p) \ll 1 \\ &\propto r^{-2-(1-\beta)(\gamma-1)\chi^{-1}} p^{-\gamma+\alpha(\gamma-1)\chi^{-1}} \\ &\quad \text{if } 1 \ll V_{\rm sw} r/K \ll \left(r/r_s\right)^{(2/3)\chi} \\ &\propto r^{-(2\gamma+4)/3} p^{-\gamma} \\ &\quad \text{if } V_{\rm sw} r/K \gg \left(r/r_s\right)^{(2/3)\chi}. \end{aligned} \quad (17)$$

Equation (17) shows that the differential fluence spectrum of SEPs arising from a power-law source injected near the Sun exhibits at 1 AU approximately three distinctive power laws for different energy ranges. A high-energy spectral break occurs at $V_{\rm sw} r/K \sim 1$ owing to the transition from a higher-energy regime ($V_{\rm sw} r/K \ll 1$), where particles diffuse out so fast that the effect of adiabatic cooling is negligible, to a lower-energy regime ($V_{\rm sw} r/K \gg 1$), where adiabatic deceleration becomes important. The solution also predicts a low-energy spectral break at $V_{\rm sw} r/K \sim (r/r_s)^{(2/3)\chi}$, below which solar wind convection dominates diffusion in interplanetary transport since particles satisfying $V_{\rm sw} r/K \gg (r/r_s)^{(2/3)\chi}$ are frozen into the solar wind once being injected at r_s.

We compute dF/dE numerically using Equations (11), (13), and (14) and compare the results with our analytical predictions. Figure 1 is the log–log plot of dF/dE versus E/E' for $\eta = 1.5$, $\gamma = 4$, and three values of r_s/r. The constant E' satisfies $V_{\rm sw} r/K(r, E') = 1$. The quantity dF/dE is normalized such that $dF/dE = 1$ at $E/E' = 1$, the position of which is denoted in the figure by an upward-pointing arrow. The downward-pointing arrows denote the energies at which $V_{\rm sw} r/K = (r/r_s)^{(2/3)\chi}$, i.e., $E/E' = (r_s/r)^{(4/3)\chi\alpha^{-1}}$, for the three choices of r_s/r. The dashed lines indicate the spectral slopes given by Equation (17). There is general agreement between the numerical and the analytical results for $V_{\rm sw} r/K \ll 1$ and $V_{\rm sw} r/K \gg (r/r_s)^{(2/3)\chi}$. In the intermediate energy range, it is not surprising to see worsening agreement for larger values of r_s/r since the analytical approximation in Equation (35) relies on the integral being dominated by the integrand evaluated over $[g_1, g_2]$, where $(r_s/r)^{(2/3)\chi} \ll g_1 < g_2 \ll 1$. As r_s/r becomes larger, the assumption has increasingly poor validity owing to the shrinkage of the interval $[g_1, g_2]$.

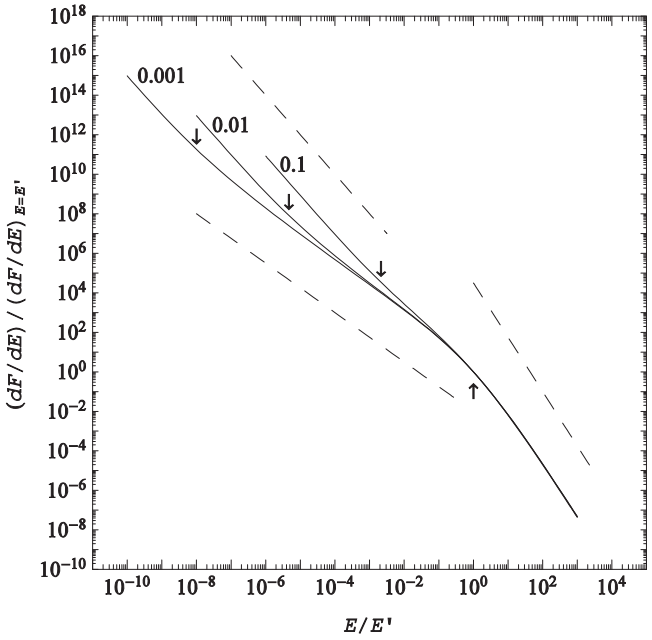

Figure 1. Normalized differential fluence vs. E/E' for three values of r_s/r as indicated, and for representative parameters listed in the text. The upward-pointing arrow indicates the energy at which $V_{\rm sw} r/K = 1$. The downward-pointing arrows indicate the energies at which $V_{\rm sw} r/K = (r/r_s)^{(2/3)\chi}$ for the three choices of r_s/r. The dashed lines show the spectral slopes of the analytical predictions.

We now estimate the valid energy range of our model. We define the event-integrated differential anisotropy as $A = 3S(v\overline{f})^{-1}$, where S, the radial differential (in p) flux density integrated over the SEP event, is given by $S = -3^{-1} V_{\rm sw} p(\partial\overline{f}/\partial p) - K(\partial\overline{f}/\partial r)$ (Gleeson & Axford 1967). Using $dF/dE = p^2\overline{f}$, we rewrite A as

$$A = -\left(\frac{V_{\rm sw}}{v}\right)\left[\frac{p}{(dF/dE)}\frac{\partial(dF/dE)}{\partial p} - 2\right] - \frac{3K}{v(dF/dE)}\frac{\partial(dF/dE)}{\partial r}. \quad (18)$$

Taking $dF/dE \propto r^{-\beta_0} p^{-\alpha_0}$ with α_0 and β_0 positive constants, we find $A = (2 + \alpha_0) V_{\rm sw} v^{-1} + \beta_0 \lambda_{\rm MFP} r^{-1}$. We note that $\lambda_{\rm MFP}(\propto p^{\alpha-1} r^{\beta})$ increases with increasing v following our choice of $1 < \eta < 2$ ($1 < \alpha < 2$). Therefore, A first decreases with increasing v as $A \approx (2 + \alpha_0) V_{\rm sw} v^{-1}$ for $V_{\rm sw} r/K \gg 1$ and then increases as $A \approx \beta_0 \lambda_{\rm MFP} r^{-1}$ for $V_{\rm sw} r/K \ll 1$. Within the framework of Equation (9), A must satisfy $|A| \ll 1$. Therefore, the validity of Equation (17) is constrained to energies from $V_{\rm sw} v^{-1} \ll 1$ to $\lambda_{\rm MFP} r^{-1} \ll 1$ approximately. The large A at low energies is due to the motion of the observer relative to the reference frame of the solar wind in which ion distributions are nearly isotropic. At high energies ($V_{\rm sw} r/K \ll 1$), the proportionality between A and $\lambda_{\rm MFP}$ arises from the fact that particles

can scatter across the surface at r multiple times through diffusive transport and that the number of crossings depends inversely on $\lambda_{\rm MFP}$.

We can quantitatively relate the number of crossings to $A(r, p)$ in the energy regime $V_{\rm sw}r/K \ll 1$, where the adiabatic energy loss of particles is negligible. We define $N_C(r, r_0, p_0)$ as the number of crossings at r by a particle injected at r_0 with momentum magnitude p_0. With our spherically symmetric model, we can obtain N_C by injecting "1" monoenergetic particle at r_0 and integrating dF/dE over all energies and over the spherical surface at r. The event-integrated distribution function of such a "single" particle is given by the Green's function G in Equation (10). Using $dF/dE = p^2G$, we have

$$N_C(r, r_0, p_0) = 16\pi^2 r^2 \int_0^{+\infty} p^2 G(r, p; r_0, p_0) v dp. \quad (19)$$

We note that, owing to adiabatic deceleration in the solar wind, the particle in principle suffers energy loss and crosses the surface each time with different remaining energy. However, for high-energy particles whose energy losses are negligible, a particularly simple expression of G obtains by retaining only the diffusion term on the left-hand side of Equation (10), which yields

$$-\frac{1}{r^2}\frac{\partial}{\partial r}\left(K_0 p^\alpha r^{\beta+2}\frac{\partial G}{\partial r}\right) = \frac{\delta(p - p_0)\delta(r - r_0)}{16\pi^2 r_0^2 p_0^2}. \quad (20)$$

With the same boundary conditions as Equation (10), the solution of Equation (20) is $G = (\beta + 1)^{-1}\delta(p - p_0)/\left(16\pi^2 K_0 p_0^{\alpha+2} r_0^{\beta+1}\right)$ for $r < r_0$ and $G = (\beta + 1)^{-1}\delta(p - p_0)/\left(16\pi^2 K_0 p_0^{\alpha+2} r^{\beta+1}\right)$ for $r > r_0$. We readily obtain from Equation (19) that for $r > r_0$

$$N_{CD}(r, p) = 3(\beta + 1)^{-1} r \lambda_{\rm MFP}^{-1}, \quad (21)$$

where we have replaced p_0 by p since there is no energy loss. The additional subscript "D" refers to this simplified scenario where diffusion dominates solar wind convection. Note that $N_{CD}(r, p)$ does not depend on r_0 and has a direct bearing on $A(r, p)$. From Equations (17) and (18) we have $A \approx (\beta + 1)\lambda_{\rm MFP} r^{-1}$ for $V_{\rm sw}r/K \ll 1$, which satisfies approximately $A = 3/N_{CD}$. We note that the number of crossings at r of a given energetic particle in an SEP event must be an odd integer for the particle to eventually diffuse or be convected out. Equations (19) and (21) shall be interpreted as the average number of crossings within the framework of Equation (9).

At even higher energies where the condition $\lambda_{\rm MFP} r^{-1} \ll 1$ breaks down, Equation (9) is not a valid description of the event-integrated distribution function. If $\lambda_{\rm MFP} r^{-1} \gg 1$, all the particles stream out of the inner heliosphere and cross the spherical surface at r only once. The differential fluence in this case can be calculated by conservation of particles as $(dF/dE)_S = (16\pi^2 r^2)^{-1} dN/dE$, where the subscript "$S$" refers to the streaming particles. Using $\int_0^r dr' \int_0^p dp' U(r', p') = N$ and $U(r, p) \propto p^{-\gamma}\delta(r - r_s)$, we obtain for $r > r_s$

$$(dF/dE)_s = \left(16\pi^2 r^2\right)^{-1}(dp/dE)\int_0^r dr' U(r', p) \propto p^{-\gamma-1} r^{-2}. \quad (22)$$

We now address the relation between $(dF/dE)_S$ and $dF/dE \propto p^{-\alpha-\gamma} r^{-1-\beta}$ as given by Equation (17) for $V_{\rm sw}r/K \ll 1$. It can be readily verified that $dF/dE \propto (dF/dE)_S N_{CD}$, where $N_{CD}(\propto p^{1-\alpha} r^{1-\beta})$ is given by Equation (21); the spectrum of the nearly isotropic particles in the energy range $V_{\rm sw}r/K \ll 1$ is softer than the spectrum of the streaming particles due to the multiple-crossing effect.

3. FITTING THE SELECTED WESTERN GLE EVENTS OF SOLAR CYCLE 23 WITH THE MODEL

Despite the fact that the proton differential fluence spectra of all 16 GLEs in Solar Cycle 23 can be well fitted by the double power-law form of Equation (1) from 0.1 MeV to 500–700 MeV, their relative element abundances and spectral properties exhibit systematic variations according to the event source region. We note that the average 5–12 MeV/nuc Fe/O value for large SEP events is 0.134 (Reames 1995). It can be seen from Table 1 that near-central meridian GLEs tend to be Fe-poor (Fe/O < 0.134) at tens of MeV/nuc and have particularly steep high-energy spectral slopes (large γ_2); both features are indicators of the strong influence of interplanetary shocks and in situ shock-accelerated populations (Cane et al. 2003, 2006). We do not attempt to account for the spectral features of the near-central meridian events with our model since these events are probably dominated at the break energy by diffusive shock acceleration in interplanetary space, which does not satisfy $r_s/r \ll 1$. We shall discuss the formation of the double power-law spectra in near-central meridian events in Section 4.

Among the 16 GLEs, nine events have Fe/O > 0.134 in both the 12–45 MeV/nuc and 45–80 MeV/nuc intervals. They are also identified by Cane et al. (2010) as Fe-rich events with minor influence of a shock-associated enhancement for protons of tens of MeV. For these events, it is reasonable to posit that the observed spectral break occurs at $V_{\rm sw}r/K \sim 1$, and that the spectral slopes γ_1 and γ_2 are correspondingly given by the analytical predictions in Equation (17) for $1 \ll V_{\rm sw}r/K \ll (r/r_s)^{(2/3)\chi}$ and $V_{\rm sw}r/K(r, p) \ll 1$. We shall confirm this hypothesis a posteriori. Following the choice of parameters in Figure 1, we find that the low-energy spectral break $V_{\rm sw}r/K = (r/r_s)^{(2/3)\chi}$ occurs at $E/E' = 4.6 \times 10^{-6}$ for $r_s/r = 0.01$ and at $E/E' = 2.2 \times 10^{-3}$ for $r_s/r = 0.1$. The quantity E' ranges from ~3 to ~30 MeV in the nine selected events. Thus, the predicted low-energy spectral break is not observed in the energy domain of the double power-law spectrum presumably because it occurs below 0.1 MeV.

Following Equation (17), we determine η and γ for the nine selected GLEs by requiring $\gamma_1 = [\gamma - (3 - \eta)(\gamma - 1)(2\eta)^{-1}]/2$ and $\gamma_2 = (3 - \eta + \gamma)/2$. The wave spectral index η must satisfy $1 < \eta < 2$, the prerequisite for the calculations in Section 2. The proton source spectral index, $\gamma = 3X(X - 1)^{-1} - 2$, should satisfy $\gamma > 2$ since the shock compression ratio $X < 4$. For a given pair of γ_1 and γ_2, there are two solutions of η and γ, but only one of them meets the conditions mentioned above. We use the qualified solution to derive X. We estimate the Alfvén Mach number using $M_{A\perp} = \sqrt{X(X + 5)/[2(4 - X)]}$, which applies for a perpendicular shock in the limiting case that the plasma beta vanishes. We also estimate the mean free path $\lambda_{\rm MFP}$ for protons of the break energy E_0 by taking $V_{\rm sw}r/K(E_0, r) = 1$ at $r = 1$ AU. We take

Table 2
Parameters Determined for the Nine Selected GLE Events

Date	η	α	β	γ	X	$M_{A\perp}$	λ_{MFP}[a](AU)
1997 Nov 06	1.978	1.022	−0.956	3.86	2.05	1.93	9.08E-03
1998 May 02	1.988	1.012	−0.976	4.65	1.82	1.69	8.13E-03
1998 May 06	1.311	1.689	0.378	3.47	2.21	2.11	4.45E-02
2001 Apr 15	1.765	1.235	−0.530	3.24	2.33	2.26	2.16E-02
2001 Apr 18	1.671	1.329	−0.342	3.69	2.12	2.00	1.95E-02
2001 Dec 26	1.557	1.443	−0.114	4.84	1.78	1.65	1.54E-02
2002 Aug 24	1.445	1.555	0.110	4.24	1.92	1.79	2.28E-02
2005 Jan 20	1.530	1.470	−0.060	2.81	2.66	2.76	3.03E-02
2006 Dec 13	1.256	1.744	0.488	3.10	2.43	2.40	5.00E-02

Note.
[a] For protons of E_0 at 1 AU.

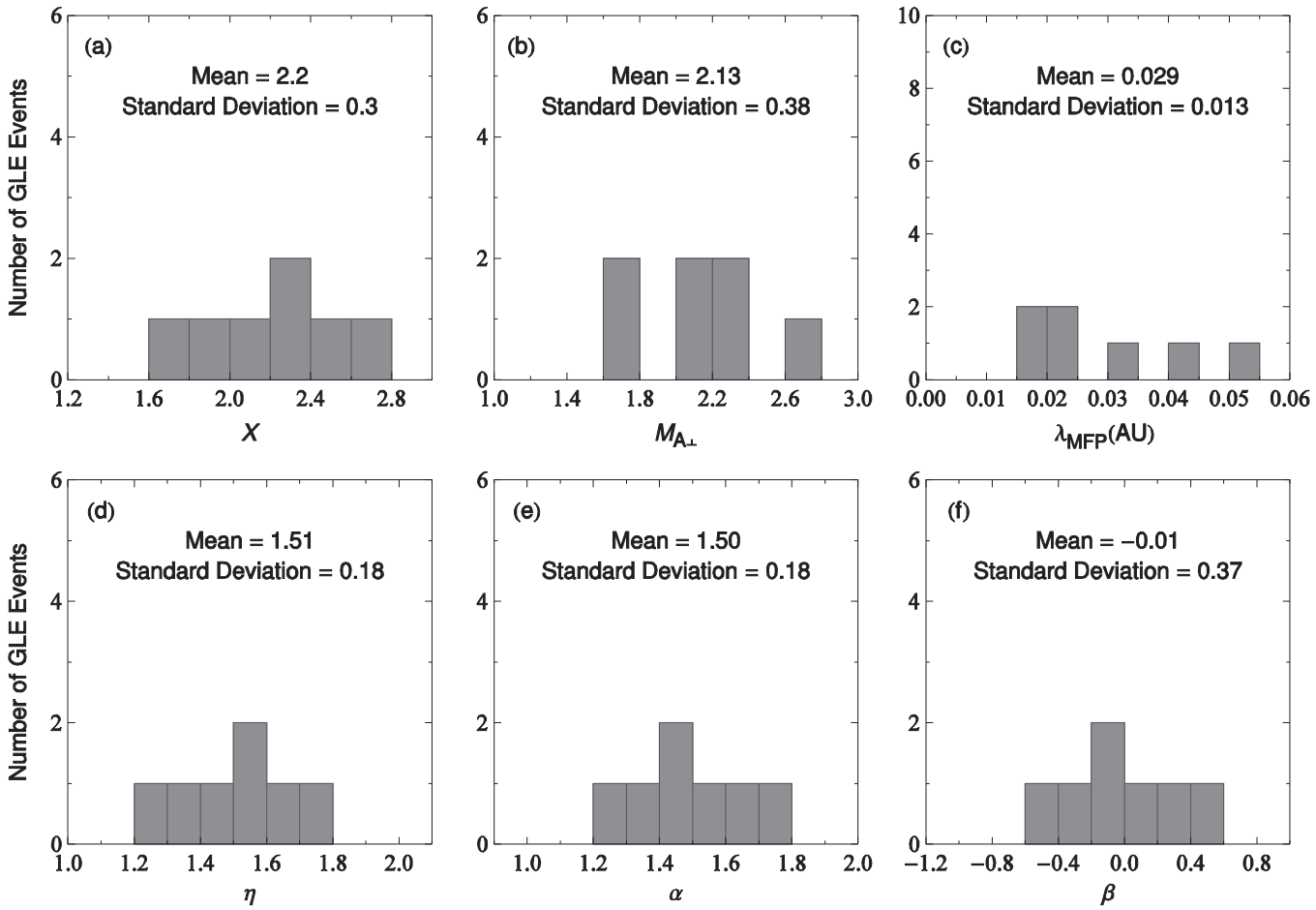

Figure 2. Histograms of (a) X, (b) $M_{A\perp}$, (c) λ_{MFP}, (d) η, (e) α, and (f) β determined for seven of the 16 GLE events of Solar Cycle 23. The radial scattering mean free path is for protons of the break energy E_0 at 1 AU.

V_{sw} to be 400 km s^{-1}. These parameters, determined for each selected event, are summarized in Table 2.

In Figure 2 we present the histograms of X, $M_{A\perp}$, λ_{MFP}, η, α, and β, for seven of the nine events in Table 2. The 1997 November 6 and 1998 May 2 events are not included in the histogram since the observed spectral properties and the derived transport parameters of them deviate obviously from the remaining events. The average value of η for the seven events is close to 5/3, the Kolmogorov spectral index. Since the Alfvén speed is much faster in the low corona than at 1 AU, it is not surprising that the average shock compression ratio is 2.2, not as large as what is expected for a strong CME-driven shock at 1 AU. It is difficult to give an estimate of the Alfvén Mach number near the Sun since both the CME speed and the Alfvén speed vary rapidly with height within a few solar radii of the photosphere. If we consider a typical GLE event where a CME accelerates from ∼800 km s^{-1} at the type II onset to its maximum speed ∼2000 km s^{-1} before the deceleration starts (Gopalswamy et al. 2012), the Alfvén Mach number is between 1.6 and 4 for a characteristic Alfvén speed ∼500 km s^{-1} near the Sun. The average value of λ_{MFP} is ∼0.03 AU for protons of ∼10 MeV at 1 AU, consistent with our scatter-dominated

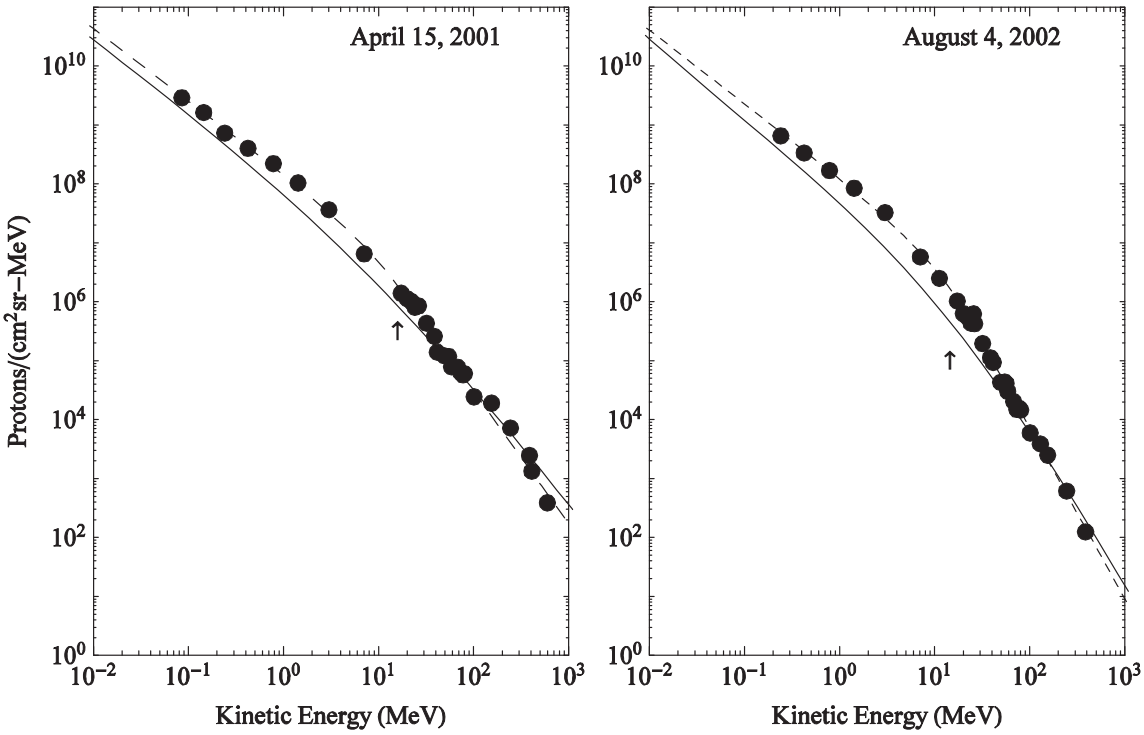

Figure 3. Numerically calculated dF/dE (solid curves) compared with observations of the 2001 April 15 and the 2002 August 4 events. In both panels, the dashed line shows the best-fit Band function for the event. The upward-pointing arrow indicates the break energy E_0. The numerical solution of dF/dE is normalized to have the same value as the Band function at $E = 100$ MeV. The data were presented in Mewaldt et al. (2012). The specific data values were provided by R. A. Mewaldt (2015, personal communication).

transport model that requires $\lambda_{\rm MFP} r^{-1} \ll 1$. The "Palmer consensus" (Palmer 1982) range for the scattering mean free path parallel to the Archimedes spiral field is $\lambda_\parallel = 0.08$–0.3AU for particles over a wide range of rigidity (5×10^{-4}–5 GV) at 1 AU. Since we have assumed a radial magnetic field, $\lambda_{\rm MFP}$ is the radial mean free path and is usually related to $\lambda_\parallel$ by $\lambda_\parallel = \lambda_{\rm MFP}/\cos^2\phi$, where $\phi(r)$ is the angle between the radial direction and the spiral field direction. We take $\cos^2\phi = 1/2$ at 1 AU and obtain $\lambda_\parallel \sim 0.06$ AU. Though slightly smaller than the lower limit of the Palmer consensus, the derived $\lambda_\parallel$ is not unreasonable for the seven selected GLEs, which, compared to ordinary SEP events, have apparently longer acceleration duration and larger event fluence that may introduce enhanced turbulence in interplanetary space. Wanner & Wibberenz (1993) showed that, depending on the momentary fluctuation levels in the interplanetary field, mean free paths can easily vary by a factor of 10 from quiet periods with little turbulence to periods with enhanced turbulence. Given the simplicity of the model, we are satisfied that the fit parameters are generally in reasonable ranges.

We compare observations with our theoretical spectra numerically calculated using Equations (11), (13), and (14) for $r_s/r = 0.01$ and for the derived parameters listed in Table 2. The proton differential fluences measured by *ACE*/ULEIS, SAMPEX/PET, and GOES-11 during the 2001 April 15 and 2002 August 24 GLE events are shown in Figure 3 (for details, see Mewaldt et al. 2012). In both panels the best-fit Band function for the event (Mewaldt et al. 2012) is plotted as the dashed line. The upward-pointing arrow indicates the break energy E_0. The solid line shows the numerically calculated dF/dE, which is normalized to have the same value as the best-fit Band function at $E = 100$ MeV. In addition, the parameters are chosen to satisfy $V_{\rm sw} r/K = 1$ at $E = E_0$. We match the numerical solution and the Band function at $E = 100$ MeV because our calculation is based on a power-law source injected near the Sun. The solution does not attempt to capture the complexity of the extended acceleration and injection of SEPs at the expanding coronal/interplanetary shock, but should be sufficient to illustrate the effects of scatter-dominated interplanetary transport on the SEP populations that are injected early in the event. We note that both events in Figure 3 originate from the west limb of the Sun. West-limb events are presumably less influenced by interplanetary shocks than well-connected and near-central meridian GLEs since the magnetic field line connecting the observer and the shock moves rapidly toward weaker regions on the flank of the shock as the shock propagates outward.

Figure 3 shows that the observed spectra exhibit an abrupt spectral break at E_0, a feature that can be well fitted by the Band function. Our solution, instead, steepens smoothly near E_0 and therefore cannot reproduce the sharp spectral transition at E_0. However, we note that, even though both events in Figure 3 are west-limb events, the event-associated shock was detected at Earth accompanied by an enhancement of protons up to ~1 MeV. It may be the extended acceleration of energetic protons between the Sun and 1 AU that "lifts" the event fluence at low energies and causes the sharpness of the spectral transition.

In Figure 4 we compare our solutions with the observations for the 2005 January 20 and the 2006 December 13 GLE events, the CME source locations of which are W61 and W23 in solar longitude, respectively. Owing to the better magnetic connection between the observer and the nose of the shock, extended acceleration presumably plays a more crucial role in

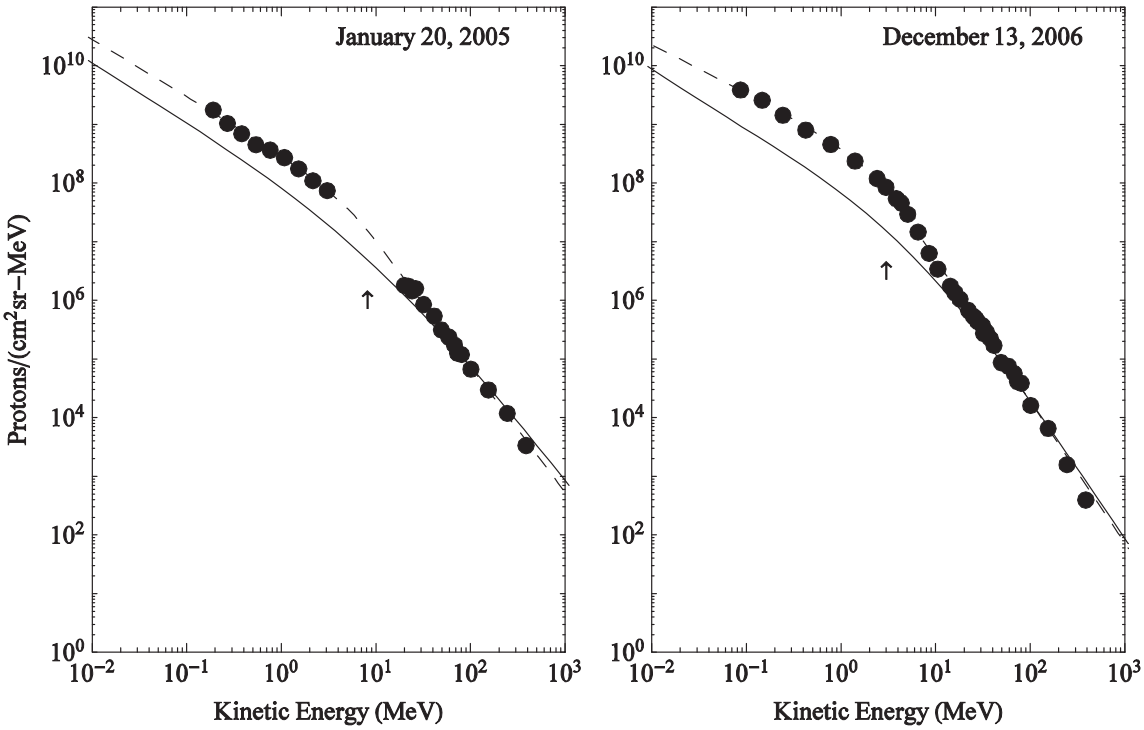

Figure 4. Numerically calculated dF/dE (solid curves) compared with observations of the 2005 January 20 and the 2006 December 13 events (see also the caption of Figure 3).

determining the event fluence at low energies for these two events than for the west-limb events in Figure 3. For instance, early in the extremely large GLE of 2005 January 20, a short plateau phase is observed, during which the intensities of protons from ∼4 to ∼20 MeV reach the low-energy streaming limit (Reames & Ng 2010). Nevertheless, the time-intensity profiles of both events in Figure 4 show a prompt onset followed by a slower decay for protons at and above tens of MeV; the high-energy spectral slope of the differential fluence spectrum is probably still a valid probe for shock acceleration near the Sun. We therefore again match our solution with the best-fit Band function at $E = 100$ MeV. The obvious elevation of the data above the theoretical spectrum at low energies may reflect the significance of extended acceleration at the traveling shock in these events.

In view of the obvious complexity of particle acceleration at an evolving CME-driven shock, involving the intrinsic time dependence of the shock strength, the magnetic obliquity of the shock front, and the geometry of the magnetic connection to Earth, it is not appropriate at this stage to perform rigorous comparisons between the model and observations. Nevertheless, the theoretical spectra in Figures 3 and 4 demonstrate that, with characteristic transport parameters, scatter-dominated interplanetary transport between the Sun and 1 AU "bends" the injected power-law source at ∼10 MeV and produces spectra that are reasonable facsimiles of those observed. On the other hand, the theoretical spectra have less sharp spectral transitions than the observations, which probably underlines the importance of extended acceleration in gradual SEP events. As we shall discuss in the next section, extended acceleration may be the dominating agent for the formation of the double power-law spectra in near-central meridian GLEs.

4. LIMITATIONS OF THE MODEL

To develop an analytically tractable model, we have made some approximations limiting the adaptability of the model:

1. The proton differential fluence given by Equation (17) is derived from a power-law source impulsively injected at $r_s \ll r$. A large gradual event usually features extended acceleration by an evolving coronal/interplanetary shock. Early in a GLE event, the power-law source is a reasonable approximation for the energy range in our study. As the CME decelerates and the shock weakens, the effects of particle losses and limited acceleration time would need to be taken into account, presumably resulting in a high-energy spectral rollover in the source spectrum. The fluence arising from an evolving shock can in principle be computed using Equation (13) and employing a source function representing diffusive shock acceleration that evolves with increasing radial distance from the Sun.
2. We have neglected the Archimedes spiral magnetic field and calculated the differential fluence with a spherically symmetric source injection, effectively ignoring drift transport and spatial diffusion perpendicular to the magnetic field. As we have addressed, during a large gradual SEP event, a spacecraft samples the corotating magnetic flux tubes that intersect the shock at a sequence of heliolongitudes, over which the shock strength may vary systematically. While the highest-energy SEPs arrive at Earth orbit promptly after being injected near the Sun, the travel-time delay of low-energy SEPs can be 1–2 days owing to the dominant role of solar wind convection in the transport of these particles to 1 AU; the azimuthal distance between the source regions of the

observed SEPs of different energies can be up to tens of degrees owing to the solar rotation rate of $\sim 13^\circ$ day^{-1}. The systematic variation of the shock strength over such a longitudinal extent becomes increasingly significant toward either flank of the shock. Thus, by assuming spherical symmetry, we probably overestimate SEP fluences of west-limb events at low energies relative to the fluences at high energies and underestimate the same ratio for near-central meridian events. It should, however, be noted that neglecting extended ion acceleration at the traveling shock of an SEP event underestimates the event fluence at low energies, which may be a compensating effect in our calculation for west-limb events. We also note that the neglected spatial diffusion normal to the field contributes to "smearing" the asymmetric distribution of SEPs in longitude.

3. Ion transport given by Equation (2) requires a smooth average interplanetary magnetic field with superimposed solar wind irregularities. Large-scale disturbances such as CMEs, shocks, and stream interaction regions complicate SEP transport. For example, in an SEP event where a preceding CME drives an additional interplanetary shock, Alfvén waves are enhanced upstream and downstream of both the interplanetary and the primary shocks, and reacceleration at multiple shocks may occur. Finally, we note that V_{sw} is taken to be constant in our calculations for simplicity. Fluctuations of the solar wind velocity may lead to stochastic acceleration of charged particles because of turbulent compressions and rarefactions in the solar wind plasma (Jokipii & Lee 2010).

We have mentioned in Section 3 that the proton fluence in near-central meridian GLEs is probably dominated at the break energy by diffusive shock acceleration in interplanetary space, which does not satisfy $r_s/r \ll 1$. The observer is not well connected to the shock front at the onset phase of a central meridian event and gradually connects closer to the nose of the shock during the $\sim$2 day period of the shock transit to 1 AU. To illustrate the effect, we neglect in Appendix C interplanetary scattering and calculate the differential fluence arising from a traveling shock that continuously injects energetic protons as it propagates from the low corona to 1 AU. We use an ad hoc source term of the Ellison–Ramaty form. The rollover energy is taken to decrease as r^{-2}. A weighting factor is introduced to suppress the contribution of the sources injected at small r, which heuristically reflects the improvement of the magnetic connection between the observer and the nose of the shock as the shock approaches 1 AU. We find that a double power-law spectrum can result from the superposition of the energetic protons injected at the evolving shock. In this case, the break energy is the rollover energy of the energetic protons injected at 1 AU. The high-energy spectral slope γ_2 increases with increasing influence of locally shock-accelerated particles. Therefore, in near-central meridian events, the break energy of the double power-law differential fluence spectrum may be just approximately the rollover energy observed in the energetic storm particle (ESP) event. The observed large γ_2 is presumably not a probe for shock acceleration near the Sun but an indicator for the significance of interplanetary shock acceleration.

5. DISCUSSION

We have presented a model for the interplanetary propagation of SEPs in large gradual events. We neglect the streaming particles and employ the Parker transport equation based on the observation that ion anisotropies are small in large gradual events after an initial increase. Our model assumes a radial magnetic field and does not include any cross-field transport. The radial diffusion coefficient is calculated with quasi-linear theory by assuming a spectrum of Alfvén waves propagating parallel to the magnetic field with an intensity determined by the WKB model.

In spite of the limitations enumerated in Section 4, the model includes the essential elements of gradual event transport: nearly isotropized ion distributions, adiabatic deceleration in a divergent solar wind, and scattering mean free paths increasing with energy. With these elements, an interesting outcome of the transport modulation is that the differential fluence spectrum arising from a power-law source injected near the Sun approximately exhibits at 1 AU three distinctive power laws for different energy domains, as illustrated in Figure 1. The spectrum in the two higher energy domains naturally reproduces the spectral features of the double power-law proton differential fluence spectra that tend to be observed in the largest SEP events. We select nine events out of the 16 GLEs during Solar Cycle 23. The selected events are mostly western events, presumably less influenced by interplanetary shocks than near-central meridian GLEs. We determine the free parameters λ_{MFP}, η, and γ for each event by fitting the observed differential fluence spectra with our model. The derived values of η and γ are generally reasonable. The derived scattering mean free paths are slightly smaller than the Palmer consensus but not unreasonable considering the importance of proton-excited waves in GLE events.

There have been relatively few published works on the origin of spectral breaks in double power-law spectra. Li et al. (2005a) introduced a loss term f/τ in the Parker equation with τ the timescale of particle leakage upstream of a shock. They argued that if the "escaping effect" sets in suddenly above a characteristic energy so that the ratio of the acceleration timescale τ_{acc} to τ has a steplike feature as a function of rigidity, a "broken" power-law spectrum can be formed. A weakness of their model is the artificial steplike rigidity dependence of τ_{acc}/τ. Ion distributions upstream of a stationary planar shock should be determined by the diffusion coefficient in the turbulent foreshock where the proton-excited wave intensity dominates the ambient wave intensity. At high energies where the wave enhancement at the resonant frequencies is not sufficiently large to promote effective diffusive shock acceleration, the diffusion coefficient increases sufficiently rapidly with distance upstream of the shock and leads to a nonvanishing escaping particle flux in the upstream direction. The p-dependence of the diffusion coefficient determines the p-dependence of the ion escape rate, which eventually determines the spectrum of the shock-accelerated ions. Since the diffusion coefficient is generally an increasing function of p, it can be shown that the upstream escape of particles introduces an exponential rollover rather than a "broken" power-law spectrum (Lee 2005).

Tylka & Lee (2006) considered diffusive shock acceleration at a traveling shock with an evolving angle between the shock normal and the upstream magnetic field. They used the Ellison–Ramaty form for the differential intensity of the shock-

accelerated ions and specified the dependence of the rollover energy on the shock obliquity based on the work of Lee (2005). The dependence includes the reduction of the ion escape rate from the shock by scattering parallel to the oblique magnetic field and reflects the reduced timescale for acceleration at quasi-perpendicular shocks. By averaging the differential intensity over the shock normal angle, they found that SEPs accelerated at an evolving quasi-perpendicular shock can have spectra of a double power-law form. Many features of the model are somewhat primitive and need to be improved to be valid in a more general situation. However, we note that the critical assumptions of the model have been verified by numerical simulations (Sandroos & Vainio 2007).

Our work provides an alternative explanation for the origin of the double power-law spectra in large gradual events. We show that a double power-law spectrum can be produced naturally through transport modulation of a power-law source without introducing further mechanisms. Our work makes no attempt to rule out other possibilities, as we have discussed in the section concerning the limitations of the model. We acknowledge the importance of extended acceleration at the traveling shock and consider it to be a controlling factor for the formation of the double power-law spectra in near-central meridian GLEs. It is certainly possible that the double power-law spectra in large gradual events reflect particle anisotropy/escape and/or the evolving obliquity of the traveling shocks.

According to our model, the observed double power-law differential fluence spectrum breaks at $V_{sw}r/K \sim 1$; therefore, break energies of different species can be scaled by the charge-to-mass ratio of ions as $(Q/M)^P$, where

$$P = 2(2 - \eta)/(3 - \eta). \tag{23}$$

For $1.4 < \eta < 1.9$, characteristic values of ambient solar wind turbulence, we find $0.18 < P < 0.75$. The Q/M dependence of spectral breaks has been ascribed to the "equal diffusion coefficient" condition for ion escape upstream of the foreshock (Cohen et al. 2005; Mewaldt et al. 2005). Cohen et al. (2005) proposed that SEP spectra break at the same value of the diffusion coefficient. They derived the same expression for P as Equation (23) but with η the spectral index of the proton-excited wave intensity in the turbulent sheath adjacent to the shock. Li et al. (2005b) predicted $P = 2$ by assuming a discontinuity ($\eta = -\infty$) in the wave spectrum at the resonant wavenumber where the spectral break occurs. Li et al. (2009) later introduced shock obliquity and perpendicular diffusion to the ion escape picture to explain the observed values of P that range from ~0.2 to ~1.8. Our model does not address how the rollover energies of different species are formed and organized in diffusive shock acceleration. However, we have demonstrated that the equal diffusion coefficient condition and the observed small values of P follow naturally if the spectral breaks are caused by scatter-dominated interplanetary transport.

In summary, we have analytically examined the effects of scatter-dominated interplanetary transport on the spectral properties of the differential fluence of large gradual SEPs using the Parker transport equation and a power-law source injected near the Sun. The model is generally successful in accounting for the double power-law proton spectra of the western GLEs in Solar Cycle 23. Our work does not address other factors in shaping SEP distribution functions but shows that transport effects are important in the interpretation of SEP spectra observed in large gradual events. Finally, we note that, for an impulsive injection of SEPs at $r_s \ll r$, our model predicts two spectral breaks for the differential fluence at $V_{sw}r/K\,(r, p) \sim 1$ and $V_{sw}r/K\,(r, p) \sim (r/r_s)^{(2/3)\chi}$, where χ is defined in Equation (11) as $\chi = \alpha + (3/2)(1 - \beta)$. As an observer moves closer to the source, the spectral break at $V_{sw}r/K\,(r, p) \sim 1$ shifts to lower energies, whereas the low-energy spectral break shifts to higher energies. *Solar Orbiter* and *Solar Probe* will be launched near the end of this decade. It will be very interesting to observe SEP events and explore particle acceleration close to the Sun.

The authors wish to acknowledge particularly helpful conversations with Dick Mewaldt and his providing us the data for the 16 GLE events. We also acknowledge the supportive atmosphere of the NASA LWS Team lead by Nat Gopalswamy to investigate extreme SEP variability. This work was supported, in part, by NASA LWS TR&T grant NNX11AO97G and by NASA SR&T grant NNX12AB32G.

APPENDIX A
SCATTER-DOMINATED INTERPLANETARY TRANSPORT

With a constant radial solar wind speed V_{sw} and a radial ambient interplanetary magnetic field, the evolution of the gyrotropic phase-space density $f(r, p, \mu, t)$ on a radial magnetic flux tube is governed by the focused transport equation incorporating solar wind convection, adiabatic deceleration, magnetic focusing, and pitch angle scattering (Roelof 1969; Earl 1981; Ruffolo 1995; Isenberg 1997),

$$\frac{\partial f}{\partial t} + (\mu v + V_{sw})\frac{\partial f}{\partial r} - \frac{1 - \mu^2}{r}V_{sw}p\frac{\partial f}{\partial p} + \frac{1 - \mu^2}{r}(\mu V_{sw} + v)\frac{\partial f}{\partial \mu} = \frac{\partial}{\partial \mu}\left[(1 - \mu^2)D_{\mu\mu}\frac{\partial f}{\partial \mu}\right]. \tag{24}$$

Note that r and t are measured in the fixed frame of the Sun, whereas v, p, and μ are measured in the solar wind frame.

We define dimensionless variables $\hat{t} = t/T_s$, $\hat{r} = r/R_s$, and $\hat{D}_{\mu\mu} = D_{\mu\mu}/D_{\mu\mu s}$, where T_s, R_s , and $D_{\mu\mu s}$ are scales for t, r, and $D_{\mu\mu}$, respectively. Then Equation (24) becomes

$$\frac{1}{D_{\mu\mu s}T_s}\frac{\partial f}{\partial \hat{t}} + \frac{V_{sw}}{R_s D_{\mu\mu s}} \times \left(\frac{\partial f}{\partial \hat{r}} - \frac{1 - \mu^2}{\hat{r}}\frac{\partial f}{\partial \ln p} + \frac{1 - \mu^2}{\hat{r}}\mu\frac{\partial f}{\partial \mu}\right) + \epsilon\left(\mu\frac{\partial f}{\partial \hat{r}} + \frac{1 - \mu^2}{\hat{r}}\frac{\partial f}{\partial \mu}\right) = \frac{\partial}{\partial \mu}\left[(1 - \mu^2)\hat{D}_{\mu\mu}\frac{\partial f}{\partial \mu}\right], \tag{25}$$

where $\epsilon = v/(R_s D_{\mu\mu s})$. Since we are considering scatter-dominated transport, ϵ satisfies $\epsilon \ll 1$. In addition, we consider SEPs characterized by particle speeds $v \gg V_{sw}$ and require $V_{sw}/v \sim \epsilon$, and therefore $V_{sw}(R_s D_{\mu\mu s})^{-1} \sim \epsilon^2$. We shall see later that particles have a convective-diffusive behavior in scatter-dominated transport with a convection speed V_{sw} and a diffusion coefficient $K \sim v^2/D_{\mu\mu s}$. The quantity T_s is

characterized by $T_s \sim R_s^2/K$ if diffusion dominates convection and by $T_s \sim R_s/V_{sw}$ if the reverse is true. It can be readily verified that in both cases $1/(D_{\mu\mu s}T_s) \sim \epsilon^2$.

We expand f in a power series in ϵ as

$$f(r, p, \mu, t) = f_0 + \epsilon f_1 + \epsilon^2 f_2 + \ldots . \quad (26)$$

Substituting Equation (26) into (25), we find at leading order in ϵ that f_0 is independent of μ. At the first order we obtain

$$\mu\frac{\partial f_0}{\partial \hat{r}} = \frac{\partial}{\partial \mu}\left[\left(1-\mu^2\right)\hat{D}_{\mu\mu}\frac{\partial f_1}{\partial \mu}\right]. \quad (27)$$

Equation (27) can be integrated over μ twice to yield f_1 as

$$f_1 = -\frac{1}{2}\frac{\partial f_0}{\partial \hat{r}}\int_{-1}^{\mu}\frac{d\mu'}{\hat{D}_{\mu\mu}(\mu')} + c\left(\hat{r}, p, t\right), \quad (28)$$

where $c(\hat{r}, p, t)$ is an integration constant. At the second order in ε, Equation (25) becomes

$$\begin{aligned}&\frac{1}{D_{\mu\mu s}T_s}\frac{\partial f_0}{\partial \hat{t}} + \frac{V_{sw}}{R_s D_{\mu\mu s}}\left(\frac{\partial f_0}{\partial \hat{r}} - \frac{1-\mu^2}{\hat{r}}\frac{\partial f_0}{\partial \ln p}\right)\\ &\quad + \epsilon^2\left(\mu\frac{\partial f_1}{\partial \hat{r}} + \frac{1-\mu^2}{\hat{r}}\frac{\partial f_1}{\partial \mu}\right)\\ &\quad = \epsilon^2\frac{\partial}{\partial \mu}\left[\left(1-\mu^2\right)\hat{D}_{\mu\mu}\frac{\partial f_2}{\partial \mu}\right]. \quad (29)\end{aligned}$$

After substituting Equation (28) into (29), we integrate over μ to obtain

$$\begin{aligned}&\frac{\partial f_0}{\partial t} + V_{sw}\frac{\partial f_0}{\partial r} - \frac{1}{r^2}\frac{\partial}{\partial r}\left[r^2\left(\frac{v^2}{8}\int_{-1}^{1}d\mu\frac{1-\mu^2}{D_{\mu\mu}}\right)\frac{\partial f_0}{\partial r}\right]\\ &\quad - \frac{2V_{sw}}{3r}p\frac{\partial f_0}{\partial p} = 0, \quad (30)\end{aligned}$$

where we have used the fact that $c(\hat{r}, p, t)$ is independent of μ. It is interesting to note that the diffusion term in Equation (30) results from the integration over μ of the last two terms on the left-hand side of Equation (29), which shows that magnetic focusing contributes to the diffusive flux of scatter-dominated particles.

APPENDIX B
DIFFERENTIAL FLUENCE SPECTRUM: APPROXIMATE SOLUTION

We simplify Equation (16) in a certain region $[g_1, g_2]$ containing the point g_0 where the integrand is maximized. Instead of obtaining g_0 by differentiating the integrand in Equation (16), we simplify the integrand with prescribed values of g_0 and then differentiate the simplified integrand to verify our presumptions. Three situations, $g_0 \approx 1$, $(r_s/r)^{(2/3)\chi} \ll g_0^{\chi} \ll 1$, and $g_0 \approx (r_s/r)^{2/3}$, are dealt with separately.

B.1. $g_0 \approx 1$

Since we are simplifying Equation (16) in a narrow region containing g_0, we take g as $g = 1-\zeta$, where $0 < \zeta \ll 1$. We expand $1-g^{\chi}$ to the first order in ζ and set $\zeta = 0$ in all the other factors. The quantity $(r_s/r)^{1-\beta}$ in the exponential function is dropped because we are calculating dF/dE at 1 AU. Additionally, we apply the small argument expansion to the Bessel function as $I_{(1+\beta)/(1-\beta)}(\xi) \propto \xi^{(1+\beta)/(1-\beta)}$, the validity of which will be addressed later. Then Equation (16) is simplified as

$$\begin{aligned}dF/dE &\propto r^{-(1+\beta)/2}p^{-\alpha-\gamma}\int_{g_1}^{g_2}dg(1-g)^{-1}\\ &\quad\times I_{\frac{1+\beta}{1-\beta}}\left(D\chi^{-1}(1-g)^{-1}\right)\exp\left(-C\chi^{-1}(1-g)^{-1}\right)\\ &\propto r^{-1-\beta}p^{-\alpha-\gamma}\int_{x(g_1)}^{x(g_2)}dx x^{-2/(1-\beta)}\exp\left(-x^{-1}\right), \quad (31)\end{aligned}$$

where $x = \chi C^{-1}\zeta = (3/2)(1-\beta)^2 K(V_{sw}r)^{-1}\zeta$. If $x^{-2/(1-\beta)}\exp(-x^{-1})$ decays rapidly as x deviates from $x(g_0)$, the integral in Equation (31) is dominated by the integrand evaluated near $x(g_0)$; the space and momentum dependence of the integral is less crucial. Thus, we obtain $dF/dE \propto r^{-1-\beta}p^{-\alpha-\gamma}$. We compare the analytical result with the numerical calculations in Section 2.

The validity of Equation (31) is restricted by the approximations made in the derivation. It can be readily shown that the integrand $x^{-2/(1-\beta)}\exp(-x^{-1})$ is maximized at

$$\zeta = 2^{-1}(1-\beta)C\chi^{-1} = 3^{-1}(1-\beta)^{-1}V_{sw}rK^{-1}. \quad (32)$$

The presumption $g_0 \approx 1$ requires $\zeta \ll 1$, and therefore p must satisfy

$$V_{sw}r/K(r, p) \ll 3(1-\beta). \quad (33)$$

Equation (33) gives the estimated range of p for $dF/dE \propto r^{-1-\beta}p^{-\alpha-\gamma}$ to be valid. The other constraint comes from the expansion $I_{(1+\beta)/(1-\beta)}(\xi) \propto \xi^{(1+\beta)/(1-\beta)}$ that requires $0 < \xi \ll 1$. Substituting ζ as given by Equation (32) into the modified Bessel function in Equation (31), we verify that the expansion is valid if

$$\left(r_s/r\right)^{(1-\beta)/2} \ll 4^{-1}(1-\beta), \quad (34)$$

which is consistent with $r_s/r \ll 1$.

B.2. $(r_s/r)^{(2/3)\chi} \ll g_0^{\chi} \ll 1$

We still neglect the quantity $(r_s/r)^{1-\beta}$ in the exponential function and perform the small argument expansion to the modified Bessel function. In addition, we take $1-g^{\chi} = 1$ and simplify Equation (16) as

$$\begin{aligned}dF/dE &\propto r^{-(1+\beta)/2}p^{-\alpha-\gamma}\int_{g_1}^{g_2}dg g^{\alpha+\gamma+(1-3\beta)/4}\\ &\quad\times I_{\frac{1+\beta}{1-\beta}}\left(Dg^{\chi-(3/4)(1-\beta)}\right)\exp\left(-Cg^{\chi}\right)\\ &\propto r^{-2-(1-\beta)(\gamma-1)\chi^{-1}}p^{-\gamma+\alpha(\gamma-1)\chi^{-1}}\\ &\quad\times\int_{y(g_1)}^{y(g_2)}dy y^{(\gamma-1)\chi^{-1}+(1+\beta)(1-\beta)^{-1}}\exp(-y), \quad (35)\end{aligned}$$

where $y = Cg^{\chi} = (2/3)(1-\beta)^{-2}\chi V_{sw}rK^{-1}g^{\chi}$. To obtain an analytical expression for the spectral slope, we neglect the modification introduced by the integral and take $dF/dE \propto r^{-2-(1-\beta)(\gamma-1)\chi^{-1}}p^{-\gamma+\alpha(\gamma-1)\chi^{-1}}$ approximately.

The valid range of p is constrained by the presumption $(r_s/r)^{(2/3)\chi} \ll g_0^{\chi} \ll 1$. Through differentiating the simplified

integrand in the second line of Equation (35), we obtain

$$g_0^{\chi} = \psi K \left(V_{\rm sw} r\right)^{-1}, \tag{36}$$

where $\psi = (3/4)\chi^{-1}(1-\beta)^2\varphi$ and $\varphi = 2[\chi^{-1}(\gamma-1) + (1+\beta)(1-\beta)^{-1}]$. Using $(r_s/r)^{(2/3)\chi} \ll g_0^{\chi} \ll 1$, we find

$$\psi \ll V_{\rm sw} r/K \ll \psi \left(r/r_s\right)^{(2/3)\chi}. \tag{37}$$

For representative parameters $\eta = 1.67$ and $\gamma = 4$ ($X = 2$), we find $\psi = 1.12$. Except for the extreme case of $\eta \to 1$ where $\psi \to 0$, the value of ψ is of order of magnitude unity. We therefore expect Equation (35) to be approximately correct within the energy domain $1 \ll V_{\rm sw} r/K \ll (r/r_s)^{(2/3)\chi}$. Substituting g_0 as given by Equation (36) into the modified Bessel function in Equation (35), we obtain the condition required by the small argument expansion as

$$\varphi \left(r_s/r\right)^{(1-\beta)/2} \ll g_0^{(3/4)(1-\beta)}. \tag{38}$$

Notice that condition (38) becomes poorly satisfied if $\eta \to 1$ where $\beta \to 1$ and $\varphi \to \infty$. For $\gamma = 4$ and $1.4 < \eta < 1.9$, we have $1.8 < \varphi < 5.1$. Therefore, the condition is generally consistent with $(r_s/r)^{(2/3)\chi} \ll g_0^{\chi}$ for representative parameters.

B.3. $g_0 \approx (r_s/r)^{2/3}$

We take $1 - g^{\chi} = 1$ and expand the modified Bessel function in Equation (16) for large argument as $I_{(1+\beta)/(1-\beta)}(\xi) \propto \xi^{-1/2}\exp(\xi)$, the validity of which will be justified later. Then we obtain

$$\begin{aligned} dF/dE &\propto r^{-(1+\beta)/2} p^{-\alpha-\gamma} \\ &\times \int_{g_1}^{g_2} dg g^{\alpha+\gamma+(1-3\beta)/4} I_{\frac{1+\beta}{1-\beta}}\left(D g^{\alpha+3(1-\beta)/4}\right) \\ &\exp\left\{-Cg^{\alpha}\left[g^{3(1-\beta)/2} + \left(r_s/r\right)^{1-\beta}\right]\right\} \\ &\propto r^{-(3+\beta)/4} p^{-\alpha/2-\gamma} \int_{g_1}^{g_2} dg g^{\alpha/2+\gamma-(1+3\beta)/8} \\ &\exp\left\{-Cg^{\alpha}\left[g^{3(1-\beta)/4} - \left(r_s/r\right)^{(1-\beta)/2}\right]^2\right\}. \end{aligned} \tag{39}$$

Taking $g = \theta_0 + \theta$, where $\theta_0 = (r_s/r)^{2/3}$ and $|\theta/\theta_0| \ll 1$, we expand the argument of the exponential function to second order in θ and set $\theta = 0$ in all the other factors. This yields

$$\begin{aligned} dF/dE &\propto r^{-(3+\beta)/4} p^{-\alpha/2-\gamma} \\ &\times \int_{\theta(g_1)}^{\theta(g_2)} d\theta \theta_0^{\alpha/2+\gamma-(3\beta+1)/8} \\ &\times \exp\left\{-C\theta_0^{\alpha-(1+3\beta)/2}[(3/4)(1-\beta)\theta]^2\right\} \\ &\propto r^{-(3+\beta)/4} p^{-\alpha/2-\gamma} \theta_0^{\gamma+(3\beta+1)/8} C^{-1/2} \int_{z(g_1)}^{z(g_2)} dz \exp\left(-z^2\right) \\ &\propto r^{-(2\gamma+4)/3} p^{-\gamma} \int_{z(g_1)}^{z(g_2)} dz \exp\left(-z^2\right), \end{aligned} \tag{40}$$

where $z = (3/4)(1-\beta)C^{1/2}\theta_0^{\alpha/2-(1+3\beta)/4}\theta$. Notice that the integrand in Equation (40) is a Gaussian function of z and peaks at $\theta = 0$, which is consistent with the presumption $g_0 \approx (r_s/r)^{2/3}$.

Through requiring the variance of θ/θ_0 in the Gaussian integrand of Equation (40) to be much smaller than 1, we find the valid energy range to be

$$V_{\rm sw} r/K \gg (4/3)\chi^{-1}\left(r/r_s\right)^{(2/3)\chi}. \tag{41}$$

If Equation (41) is satisfied, the integral in Equation (40) hardly changes the dependence of the differential fluence on r and p, and therefore $dF/dE \propto r^{-(2\gamma+4)/3}p^{-\gamma}$. The expansion $I_{(1+\beta)/(1-\beta)}(\xi) \propto \xi^{-1/2}\exp(\xi)$ requires $\xi \gg 1$. Substituting $g = (r_s/r)^{2/3}$ into the modified Bessel function in Equation (39), we determine the constraint on p to be

$$V_{\rm sw} r/K \gg (3/4)\chi^{-1}(1-\beta)^2\left(r/r_s\right)^{(2/3)\chi}, \tag{42}$$

which is consistent with Equation (41).

Combining Equations (31), (35), (40), and their estimated valid energy ranges as discussed previously, we obtain the approximate solution presented in Equation (17). At the highest energies ($V_{\rm sw} r/K \ll 1$), particles diffuse out so fast that adiabatic cooling is a higher-order effect for them. Within the energy domain $1 \ll V_{\rm sw} r/K \ll (r/r_s)^{(2/3)\chi}$, adiabatic cooling hardens the differential fluence spectrum since particles with a lower momentum lose a larger portion of energy through interplanetary transport. This effect is quantitatively illustrated by Equation (36), which can be rearranged to obtain $p/p_0 \propto p^{\alpha\chi^{-1}}$. Particles satisfying $V_{\rm sw} r/K \ll (r/r_s)^{(2/3)\chi}$ are frozen into the solar wind once being injected at r_s. Since these particles lose the same ratio of energy through interplanetary transport, adiabatic cooling does not harden the spectrum in the lowest energy domain.

APPENDIX C
EXTENDED DIFFUSIVE SHOCK ACCELERATION IN NEAR-CENTRAL MERIDIAN GLE EVENTS

In near-central meridian GLE events, the shock transit speed can be over 1000 km s^{-1} and the observer sees a characteristic ESP enhancement as the shock approaches Earth. We believe that diffusive shock acceleration at the interplanetary shock is an important factor that softens the high-energy spectral slope in the observed double power-law differential fluence spectra. To illustrate this behavior, we neglect interplanetary scattering and calculate the differential fluence arising from the extended injection at a traveling shock.

We reasonably assume that the source function $u_{\rm inj}$ in Equation (2) has the Ellison–Ramaty (Ellison & Ramaty 1985) form and the cutoff momentum p_c of the spectral rollover satisfies $p_c = p_{\rm 1AU} r_E r^{-1}$, where $p_{\rm 1AU}$ is the cutoff momentum observed following the arrival of the shock at $r_E = 1$AU. For nonrelativistic protons we specify $u_{\rm inj}$ as

$$\begin{aligned} u_{\rm inj}(r, p, t) = &\frac{N_{\rm sh}}{p_{\rm inj}^3}\left(\frac{p}{p_{\rm inj}}\right)^{-3X(X-1)^{-1}} \\ &\times \exp\left[-\left(\frac{pr}{p_{\rm 1AU} r_E}\right)^2\right]\delta(r - r_{\rm sh}), \end{aligned} \tag{43}$$

where $r_{\rm sh}(t)$ is the position of the traveling shock and $p_{\rm inj}$ is the proton injection momentum at the shock. The coefficient $N_{\rm sh}$, in units of ions cm^{-2} s^{-1}, is associated with the injection rate of solar wind protons into the shock acceleration process. We note that $N_{\rm sh}$ is usually assumed to satisfy $N_{\rm sh} \propto (V_{\rm sh} - V_{\rm sw})$. For

our illustrative purposes here, we take for simplicity $N_{\rm sh} = \varsigma n V_{\rm sh}$, where $V_{\rm sh}$ is the radial speed of the CME-driven shock, ς is a constant, and $n(r)$ is the number density of protons in the ambient plasma. To accommodate the spherical geometry, we take $n = n_E (r_E/r)^2$, where n_E is the proton number density at 1 AU. We also take $p_{\rm inj}$ and X to be constant. Using $U(r, p) = 16\pi^2 r^2 p^2 \int_{t_1}^{t_2} u_{\rm inj} dt$ and $dt = V_{\rm sh}^{-1} dr_{\rm sh}$, we obtain

$$U(r, p) = \frac{16\pi^2 n_E r_E^2 \varsigma}{p_{\rm inj}} \left(\frac{p}{p_{\rm inj}}\right)^{-\gamma} \exp\left[-\left(\frac{pr}{p_{\rm 1AU}\, r_E}\right)^2\right], \quad (44)$$

where $\gamma = 3X(X-1) - 2$. Note that Equations (43) and (44) are defined in the spatial domain $[r_{\rm sh}(t_1), r_{\rm sh}(t_2)]$, where the shock has formed and the diffusive acceleration remains efficient. For a central meridian GLE event, $r_{\rm sh}(t_1) \ll 1$AU and $r_{\rm sh}(t_2) > 1$AU. The source function vanishes outside of the domain.

At the onset of a central meridian event, the observer is not well connected to the shock front and records fewer high-energy protons than it does in western events. The magnetic connection between the observing spacecraft and the nose of the CME-driven shock improves with time. The proton fluence below ~1 MeV is usually dominated by the ESP enhancement prior to shock passage. To qualitatively reflect the improvement of the magnetic connection between the observer and the nose of the shock as the shock approaches 1 AU, we introduce a heuristic weighting factor $(r/r_E)^w$, where $w(>0)$ is a constant. The weighting factor suppresses the contribution of the sources injected at $r/r_E < 1$ to the event fluence. A larger w indicates a stronger influence of locally shock-accelerated particles compared to particles accelerated near the Sun. Ignoring interplanetary scattering, we obtain from Equations (22) and (44) the differential fluence at r_E

$$\begin{aligned}(dF/dE)_S &= \left(16\pi^2 r_E^2\right)^{-1} (dp/dE) \\ &\quad \times \int_{r_{\rm sh}(t_1)}^{r_E} dr_0\, U(r_0, p) \left(r_0/r_E\right)^w \\ &= \frac{\varsigma n_E r_E}{p_{\rm inj}} \left(\frac{p}{p_{\rm 1AU}}\right)^{-(w+1)} \left(\frac{p}{p_{\rm inj}}\right)^{-\gamma} \\ &\quad \times \left(\frac{dp}{dE}\right) \int_0^{pp_{\rm 1AU}^{-1}} d\rho \rho^w \exp\left(-\rho^2\right), \end{aligned} \quad (45)$$

where $\rho = pp_{\rm 1AU}^{-1} r r_E^{-1}$. Note that $(dF/dE)_S$ is the differential fluence of the streaming particles. Energy losses and the multiple-crossing effect are neglected. We consider the momentum domain $pp_{\rm 1AU}^{-1} r_{\rm sh}(t_1) r_E^{-1} \ll 1$, which is equivalent to assuming that, early in a GLE event, the high-energy rollover of the injected protons occurs at an energy much higher than the energy we consider. Notice that the lower limit of the integral in Equation (45) has been replaced by 0 since the integrand is convergent as $\rho \to 0$. If $p/p_{\rm 1AU} \ll 1$, we find $(dF/dE)_s \propto p^{-\gamma-1}$, which has the identical momentum dependence as Equation (22) since the spectral rollover does not occur in this energy domain. If $p/p_{\rm 1AU} \gg 1$, $\int_0^{p/p_{\rm 1AU}} d\rho \rho^w \exp(-\rho^2) \approx \Gamma[(w+1)/2]/2$ and $(dF/dE)_S \propto p^{-\gamma-w-2}$.

Our calculation shows that if an ESP contribution dominates the low-energy fluence, the break momentum of the double power-law spectrum is $p_{\rm 1AU}$, the rollover momentum observed in the ESP event. Following the particle escape picture proposed by Cohen et al. (2005), the rollover energy of different elements in an ESP event is expected to be scaled by the ion charge-to-mass ratio as $(Q/M)^P$ with $P = 2$ in the limiting case given by Li et al. (2005b). On the other hand, the value of P given by our model is $0.18 < P < 0.75$ for $1.4 < \eta < 1.9$. Therefore, the break energy of different elements is expected to be more sensitively dependent on Q/M in the events where the spectral break originates from local diffusive shock acceleration ($P = 2$) than in the events where the spectral break originates from scatter-dominated interplanetary transport ($0.18 < P < 0.75$).

In addition, we have demonstrated that, as the influence of locally shock-accelerated particles increases (larger w), the high-energy spectral slope γ_2 becomes steeper. The strong spectral steepening (large $\gamma_2 - \gamma_1$) and the sensitive dependence of the break energy on Q/M naturally result in a strongly decreasing Fe/O ratio above the break energy of iron. Such a feature is probably responsible for why the near-central meridian GLEs in Table 1 tend to have Fe/O < 0.134 at tens of MeV/nuc.

REFERENCES

Band, D., Matteson, J., Ford, L., et al. 1993, ApJ, 413, 281
Bell, A. R. 1978, MNRAS, 182, 147
Cane, H. V., McGuire, R. E., & von Rosenvinge, T. T. 1986, ApJ, 301, 448
Cane, H. V., Mewaldt, R. A., Cohen, C. M. S., & von Rosenvinge, T. T. 2006, JGR, 111, A06S90
Cane, H. V., Richardson, I. G., & von Rosenvinge, T. T. 2010, JGR, 115, A08101
Cane, H. V., von Rosenvinge, T. T., Cohen, C. M. S., & Mewaldt, R. A. 2003, GeoRL, 30, 8017
Cohen, C. M. S., Stone, E. C., Mewaldt, R. A., et al. 2005, JGR, 110, A09S16
Dalla, S., Marsh, M. S., Kelly, J., & Laitinen, T. 2013, JGR, 118, 5979
Earl, J. A. 1976, ApJ, 205, 900
Ellison, D. C., & Ramaty, R. 1985, ApJ, 298, 400
Gleeson, L. J., & Axford, W. I. 1967, ApJL, 149, L115
Gopalswamy, N., Xie, H., Yashiro, S., et al. 2012, SSRv, 171, 23
Gordon, B. E., Lee, M. A., Möbius, E., & Trattner, K. H. 1999, JGR, 104, 28263
Hollweg, J. V. 1973, JGR, 78, 3643
Isenberg, P. A. 1997, JGR, 102, 4719
Jokipii, J. R. 1966, ApJ, 143, 961
Jokipii, J. R. 1982, ApJ, 255, 716
Jokipii, J. R., & Lee, M. A. 2010, ApJ, 713, 475
Kahler, S. 1994, ApJ, 428, 837
Lee, M. A. 1982, JGR, 87, 5063
Lee, M. A. 1983, JGR, 88, 6109
Lee, M. A. 2005, ApJS, 158, 38
Li, G., Hu, Q., & Zank, G. P. 2005a, in AIP Conf. Proc. 781, The Physics of Collisionless Shocks, ed. G. Li, G. P. Zank & C. T. Russell (New York: AIP), 223
Li, G., Zank, G. P., & Rice, W. K. M. 2005b, JGRA, 110, 06104
Li, G., Zank, G. P., Verkhoglyadova, O., et al. 2009, ApJ, 702, 998
Marsh, M. S., Dalla, S., Kelly, J., & Laitinen, T. 2013, ApJ, 774, 4
Mason, G. M., Desai, M. I., Cohen, C. M. S., et al. 2006, ApJL, 647, L65
Mewaldt, R. A., Cohen, C. M. S., Haggerty, D. K., et al. 2008, in Proc. 30th ICRC, 1, 99
Mewaldt, R. A., Cohen, C. M. S., Labrador, A. W., et al. 2005, JGR, 110, A09S18
Mewaldt, R. A., Looper, M. D., Cohen, C. M. S., et al. 2012, SSRv, 171, 97
Neugebauer, M., & Giacalone, J. 2005, JGR, 110, A12106
Ng, C. K., & Reames, D. V. 1994, ApJ, 424, 1032
Ng, C. K., Reames, D. V., & Tylka, A. J. 1999, GeoRL, 26, 2145
Ng, C. K., Reames, D. V., & Tylka, A. J. 2003, ApJ, 591, 461
Palmer, I. D. 1982, RvGSP, 20, 335

Parker, E. N. 1965a, P&SS, 13, 9
Parker, E. N. 1965b, SSRv, 4, 666
Reames, D. V. 1990, ApJL, 358, L63
Reames, D. V. 1995, AdSpR, 15, 41
Reames, D. V. 2009, ApJ, 693, 812
Reames, D. V., & Ng, C. K. 1998, ApJ, 504, 1002
Reames, D. V., & Ng, C. K. 2010, ApJ, 723, 1286
Reames, D. V., Ng, C. K., & Berdichevsky, D. 2001, ApJ, 550, 1064
Roelof, E. C. 1969, in Lectures in High Energy Astrophysics, ed. H. Ogelmann & J. R. Wayland (Washington: GPO), 111
Ruffolo, D. 1995, ApJ, 442, 861
Sandroos, A., & Vainio, R. 2007, ApJL, 662, L127
Tan, L. C., Reames, D. Y., & Ng, C. K. 2007, ApJ, 661, 1297
Tan, L. C., Reames, D. Y., & Ng, C. K. 2008, ApJ, 678, 1471
Tylka, A. J., Boberg, P. R., McGuire, E., Ng, C. K., & Reames, D. V. 2000, in AIP Conf. Proc. 528, Acceleration and Transport of Energetic Particles Observed in the Heliosphere: ACE 2000 Symp., ed. R. A. Mewaldt et al. (New York: AIP), 147
Tylka, A. J., Cohen, C. M. S., Dietrich, W. F., et al. 2005, ApJ, 625, 474
Tylka, A. J., & Lee, M. A. 2006, ApJ, 646, 1319
Vainio, R. 2003, A&A, 406, 735
Vanio, R., Kocharov, L., & Laitinen, T. 2000, ApJ, 528, 1015
Wanner, W., & Wibberenz, G. 1993, JGR, 98, 3513
Webb, G. M., & Gleeson, L. J. 1974, PASAu, 2, 299